

## Reflectance quantities in optical remote sensing—definitions and case studies

G. Schaepman-Strub<sup>a,b,\*</sup>, M.E. Schaepman<sup>c</sup>, T.H. Painter<sup>d</sup>, S. Dangel<sup>b</sup>, J.V. Martonchik<sup>e</sup>

<sup>a</sup> Nature Conservation and Plant Ecology Group, Wageningen University and Research Centre, Bornsesteeg 69, 6708 PD Wageningen, The Netherlands

<sup>b</sup> RSL, Department of Geography, University of Zurich, Winterthurerstrasse 190, 8057 Zurich, Switzerland

<sup>c</sup> Centre for Geo-information, Wageningen University and Research Centre, 6700 AA Wageningen, The Netherlands

<sup>d</sup> National Snow and Ice Data Center (NSIDC), University of Colorado at Boulder, 449 UCB, Boulder, CO 80309-0449, United States

<sup>e</sup> Jet Propulsion Laboratory, 4800 Oak Grove Drive, Pasadena, CA 91109, United States

Received 9 May 2005; received in revised form 1 March 2006; accepted 4 March 2006

### Abstract

The remote sensing community puts major efforts into calibration and validation of sensors, measurements, and derived products to quantify and reduce uncertainties. Given recent advances in instrument design, radiometric calibration, atmospheric correction, algorithm development, product development, validation, and delivery, the lack of standardization of reflectance terminology and products becomes a considerable source of error. This article provides full access to the basic concept and definitions of reflectance quantities, as given by Nicodemus et al. [Nicodemus, F.E., Richmond, J.C., Hsia, J.J., Ginsberg, I.W., and Limperis, T. (1977). Geometrical Considerations and Nomenclature for Reflectance. In: National Bureau of Standards, US Department of Commerce, Washington, D.C. URL: <http://physics.nist.gov/Divisions/Div844/facilities/specphoto/pdf/geoConsid.pdf>.] and Martonchik et al. [Martonchik, J.V., Bruegge, C.J., and Strahler, A. (2000). A review of reflectance nomenclature used in remote sensing. *Remote Sensing Reviews*, 19, 9–20.]. Reflectance terms such as BRDF, HDRF, BRF, BHR, DHR, black-sky albedo, white-sky albedo, and blue-sky albedo are defined, explained, and exemplified, while separating conceptual from measurable quantities. We use selected examples from the peer-reviewed literature to demonstrate that very often the current use of reflectance terminology does not fulfill physical standards and can lead to systematic errors. Secondly, the paper highlights the importance of a proper usage of definitions through quantitative comparison of different reflectance products with special emphasis on wavelength dependent effects. Reflectance quantities acquired under hemispherical illumination conditions (i.e., all outdoor measurements) depend not only on the scattering properties of the observed surface, but as well on atmospheric conditions, the object's surroundings, and the topography, with distinct expression of these effects in different wavelengths. We exemplify differences between the hemispherical and directional illumination quantities, based on observations (i.e., MISR), and on reflectance simulations of natural surfaces (i.e., vegetation canopy and snow cover). In order to improve the current situation of frequent ambiguous usage of reflectance terms and quantities, we suggest standardizing the terminology in reflectance product descriptions and that the community carefully utilizes the proposed reflectance terminology in scientific publications.

© 2006 Elsevier Inc. All rights reserved.

**Keywords:** Reflectance; Terminology; Definition; Nomenclature; BRDF; Spectrodirectional; Vegetation; Snow

### 1. Introduction

Since its origins, the remote sensing community has explored the angular distribution of reflectance through field measurements, laboratory measurements, remotely sensed mea-

surements, and modeling studies. Nicodemus et al. (1977) defined a widely cited, unified approach to the specification of reflectance and proposed a nomenclature to facilitate this approach. In this work, they developed the theoretical framework for discussion of reflectance quantities, based on the concept of the bidirectional reflectance distribution function (BRDF), and presented the caveats of the connection of this framework with measurements. Reflectance nomenclature in the remote sensing and laboratory/field measurement literature has loosely followed the framework of Nicodemus et al. (1977)

\* Corresponding author. Nature Conservation and Plant Ecology Group, Wageningen University and Research Centre, Bornsesteeg 69, 6708 PD Wageningen, The Netherlands.

E-mail address: [Gabriela.Schaepman@wur.nl](mailto:Gabriela.Schaepman@wur.nl) (G. Schaepman-Strub).

and yet the caveats remain largely ignored, leaving a literature rife with loosely understood concepts and measured quantities that cannot be compared or modeled adequately due to erroneous or ambiguous nomenclature. Whereas it was hypothesized (Koestler, 1959) and later disproved (Gingerich, 2004) that Copernicus' *de Revolutionibus* (Copernicus, 1543) was not thoroughly read and understood, past and current remote sensing literature demonstrate that Nicodemus et al. (1977) has in fact been widely misunderstood, misapplied, or ignored. In this work, we extend the definition of reflectance nomenclature to its application specifically in remote sensing and field measurements, and present the implications of terminology misuse when inferring surface physical parameters. We consider a physically consistent, explicit declaration of reflectance quantities to be a prerequisite in peer-reviewed literature.

The physically based terminology proposed by Nicodemus et al. (1977) was updated and adapted to the remote sensing case by Martonchik et al. (2000), and the concept of the BRDF was then extended to horizontally heterogeneous surfaces by Snyder (2002). It was further generalized by Di Girolamo (2003) to include the area of illumination and the area of measurement as dependent variables, and thus explaining experimental results which questioned the validity of the reciprocity of the BRDF. On the practical side, recent advances in data production by the science team for the NASA Multi-angle Imaging Spectro-Radiometer (MISR) have led to a more uniform and physically consistent reflectance terminology for operational reflectance products. The MISR data products that include different reflectance quantities allow users to infer appropriate physical quantities for their investigations.

Despite these advancements, the peer-reviewed literature shows that the remote sensing community still often neglects the description of the physical conditions of measurements and the corresponding terminology of at-surface reflectance quantities. This problem comes in the form of ambiguous or erroneous usage of the terminology.

The most striking oversight by our community is that of the "measurement of the BRDF" in which neither the actual irradiance nor measured reflected field is properly directional. As Nicodemus et al. (1977) state, "The BRDF itself, as a ratio of infinitesimals, is a derivative with "instantaneous" [in angle] values that can never be measured directly."

Under natural conditions for Earth observing, the assumption of a single direction of the incident beam for all ground based, airborne, and spaceborne optical sensor measurements is invalid. Natural irradiance is composed of a direct component (non-scattered radiation) and a diffuse component scattered by the atmosphere (gases, aerosols, and clouds), and the surroundings of the observed surface. The magnitude and spectral distribution of the diffuse irradiance therefore depends on atmospheric conditions, topography, and the reflectance properties of the topography. Without correction of the diffuse component of the irradiance, observed reflectance quantities are influenced by the above effects and do not represent the desired intrinsic directional reflectance characteristics of the observed surface.

The analysis of illumination effects present in measured reflectance data is discussed in the literature (Deering & Eck,

1987; Kriebel, 1976, 1978; Liu et al., 1994; Ranson et al., 1985). Several studies have analyzed simulated reflectance data under different ratios of direct and diffuse irradiance conditions (e.g., Asrar & Myneni, 1993; Lewis & Barnsley, 1994). Lyapustin and Privette (1999) showed that the reflectance function derived from measurements performed under ambient sky conditions contains an atmospheric contribution, and therefore shows considerable shape distortions with respect to the inherent surface BRDF. Thus, experimental research on the inherent reflectance anisotropy of the observed surface requires an accurate atmospheric correction as developed by Martonchik (1994) and Lyapustin and Privette (1999).

Furthermore, the instantaneous field of view (IFOV) of the instrument may integrate over a large viewing solid angle rather than an infinitesimal differential solid angle specific to the BRDF. Thus, remote sensing measurements do not properly coincide with bidirectional reflectance quantities and resulting products should only be considered as approximations to the surface bidirectional reflectance, a fact often neglected.

Quantitative comparisons of reflectance products provided by different airborne or satellite sensor systems with inconsistent definitions or data descriptions are difficult, inaccurate, or impossible. An explicit description of irradiance conditions and sensor geometric specifications (i.e. IFOV) of the delivered at-surface reflectance products is necessary for such comparisons. This is true for discrete angular observations, as well as inferred hemispherical products such as albedo.

Given the state of terminology currently in practice, this paper first gives an extensive physical and mathematical description of different reflectance quantities and separates conceptual from measurable quantities. Based on this background, we present examples from peer-reviewed literature that exhibit frequent ambiguous or wrong usage of current reflectance terminology. We then systematically highlight differences in at-surface reflectance quantities by their definition. We focus on the geometry of the solid angle of the illumination, i.e., directional and hemispherical extent. We quantitatively compare operational MISR reflectance products with respect to the corresponding atmospheric optical depth and resulting wavelength-specific differences for selected biomes and then perform modeling studies for two significantly different natural surfaces, forest and snow. Using a variation of the direct to diffuse irradiance ratio in the corresponding radiative transfer models (i.e. Rahman–Pinty–Verstraete (RPV), Discrete Ordinate Radiative Transfer (DISORT)), we obtain quantitative results of the wavelength-dependent influence of the diffuse component on the hemispherical–directional surface reflectance, i.e., for an illumination of hemispherical extent.

## 2. Definitions

In the following, we present the definitions of most commonly used reflectance quantities, based on the initial terminology of Nicodemus et al. (1977) and Martonchik et al. (2000), using notations listed in Table 1, and present associated examples of their implementation.

Table 1  
Notations used for the definition of at-surface reflectance quantities

Symbols	
$S$	Distribution of direction of radiation
$A$	Surface area [ $\text{m}^2$ ]
$\Phi$	Radiant flux [W]
$E$	Irradiance, incident flux density; $\equiv d\Phi/dA$ [ $\text{W m}^{-2}$ ]
$L$	Radiance; $\equiv d^2\Phi/(dA \cdot \cos\theta \cdot d\omega)$ [ $\text{W m}^{-2} \text{sr}^{-1}$ ]
$M$	Radiant exitance, exitent flux density; $\equiv d\Phi/dA$ [ $\text{W m}^{-2}$ ]
$\rho$	Reflectance; $\equiv d\Phi_r/d\Phi_i$ [dimensionless]
$R$	Reflectance factor; $\equiv d\Phi_r/d\Phi_{\text{rid}}$ [dimensionless]
$\theta$	Zenith angle, in a spherical coordinate system [rad]
$\phi$	Azimuth angle, in a spherical coordinate system [rad]
$\omega$	Solid angle; $\equiv \int d\omega \equiv \int \int \sin\theta \cdot d\theta \cdot d\phi$ [sr]
$\Omega$	Projected solid angle; $\equiv \int \cos\theta \cdot d\omega \equiv \int \int \cos\theta \cdot \sin\theta \cdot d\theta \cdot d\phi$ [sr]
$\lambda$	Wavelength of radiation [nm]
$f()$	Function
<i>Sub- and superscripts</i>	
i	Incident
r	Reflected
id	Ideal (lossless) and diffuse (isotropic or Lambertian)
atm	Atmospheric
dir	Direct
diff	Diffuse
<i>Terms</i>	
BHR	BiHemispherical Reflectance
BRDF	Bidirectional Reflectance Distribution Function
BRF	Bidirectional Reflectance Factor
DHR	Directional–Hemispherical Reflectance
HDRF	Hemispherical–Directional Reflectance Factor

### 2.1. Radiance, reflectance, reflectance factors

The prerequisite for physically based, quantitative analysis of airborne and satellite sensor measurements in the optical domain is their calibration to spectral radiance. The spectral radiance is the radiant flux in a beam per unit wavelength and per unit area and solid angle of that beam, and is expressed in the SI units [ $\text{W m}^{-2} \text{sr}^{-1} \text{nm}^{-1}$ ].

The ratio of the radiant exitance ( $M$  [ $\text{W m}^{-2}$ ]) with the irradiance ( $E$  [ $\text{W m}^{-2}$ ]) results in the so-called *reflectance*. Following the law of energy conservation, the value of the reflectance is in the inclusive interval 0 to 1. The *reflectance factor* is the ratio of the radiant flux reflected by a surface to that reflected into the same reflected-beam geometry and wavelength range by an ideal (lossless) and diffuse (Lambertian) standard surface, irradiated under the same conditions. For measurement purposes, a Spectralon panel commonly approximates the ideal diffuse standard surface. Reflectance factors can reach values beyond 1, especially for strongly forward reflecting surfaces such as snow (Painter & Dozier, 2004). We assume further that an isotropic behavior implies a spherical source that radiates the same in all directions, i.e., the intensity [ $\text{W sr}^{-1}$ ] is the same in all directions, whereas the diffuse (Lambertian) behavior refers to a flat reflective surface. Consequently the intensity falls off as the cosine of the observation angle with respect to the surface normal (Lambert's law) and the radiance  $L$  [ $\text{W m}^{-2} \text{sr}^{-1}$ ] is independent of direction. However, the ratio of the radiant exitance  $M$  [ $\text{W m}^{-2}$ ]

to the radiance  $L$  [ $\text{W m}^{-2} \text{sr}^{-1}$ ] of a Lambertian surface is a factor of  $\pi$  (Palmer, 1999).

### 2.2. Conceptual and measurable reflectance quantities

We symbolize reflectance and reflectance factor as

$$\rho(S_i, S_r, \lambda) = \text{reflectance, and}$$

$$R(S_i, S_r, \lambda) = \text{reflectance factor,}$$

where  $S_i$  and  $S_r$  describe the angular distribution of all incoming and reflected radiance observed by the sensor, respectively.  $S_i$  and  $S_r$  only describe a set of angles occurring with the incoming and reflected radiation and not their intensity distributions.  $S_r$  represents a cone with a given solid angle corresponding to a sensor's instantaneous field of view (IFOV), but no sensor weight functions are included here. If the sensitivity of the sensor depends on the location within the rim of the cone, a response function should be included. When a sensor has a different IFOV for different wavelength ranges, then  $S_r$  depends on the wavelength.

The terms  $S_i$  and  $S_r$  can be expanded into a more explicit angular notation to address the remote sensing problem:

$$\rho(\theta_i, \phi_i, \omega_i; \theta_r, \phi_r, \omega_r; \lambda), \text{ and}$$

$$R(\theta_i, \phi_i, \omega_i; \theta_r, \phi_r, \omega_r; \lambda),$$

where the directions ( $\theta$  and  $\phi$  are the zenith and azimuth angle, respectively) of the incoming (subscript i) and the reflected (subscript r) radiance, and the associated solid angles of the cones ( $\omega$ ) are indicated. This notation follows the definition of a general cone.

From a physical point of view, we may define special cases of  $\rho$  and  $R$  in terms of conceptual quantities and measurable quantities. Conceptual quantities of reflectance include the assumption that the size to distance ratio of the illumination source (usually the sun or lamp) and the observing sensor is zero. They are labeled *directional* in the general terminology. Since infinitesimal elements of solid angle do not include measurable amounts of radiant flux (Nicodemus et al., 1977), and unlimited small light sources and sensor IFOVs do not exist, all measurable quantities of reflectance are performed in the *conical* or *hemispherical* domain of geometrical considerations. Thus, actual measurements always involve non-zero intervals of direction and the underlying basic quantity for all radiance and reflectance measurements is the conical case.

For surface radiance measurements made from space, aircraft or on the ground, under ambient sky conditions, the incident radiance cone is of hemispherical extent ( $\omega = 2\pi$  [sr]). The irradiance can then be divided into a direct sunlight component and a second irradiance component, namely sunlight which has been scattered by the atmosphere, the terrain, and surrounding objects, resulting in an anisotropic, diffuse illumination. Because the ratio of diffuse to direct irradiance is a function of wavelength, it highly influences the spectral dependence of directional effects as shown in the quantitative comparison section of this paper.

The above reflectance and reflectance factor definitions lead to the following special cases:

- $\omega_i$  or  $\omega_r$  are omitted when either is zero (directional quantities).
- If  $0 < (\omega_i \text{ or } \omega_r) < 2\pi$ , then  $\theta, \phi$  describe the direction of the center axis of the cone (e.g. the line from a sensor to the center of its ground field of view—conical quantities).
- If  $\omega_i = 2\pi$ , the angles  $\theta_i, \phi_i$  indicate the direction of the incoming direct radiation (e.g., the position of the sun). For remote sensing applications, it is often useful to separate the natural incoming radiation into a direct (neglecting the sun’s size) and hemispherical diffuse part. One may also include a terrain reflected diffuse component that is calculated with a topographic radiation model such as TOPORAD (Dozier, 1980). Consequently, the preferred notation for the geometry of the incoming radiation under ambient illumination conditions is  $\theta_i, \phi_i, 2\pi$ . Note that in this case,  $\theta_i, \phi_i$  describe the position of the sun and not the center of the cone ( $2\pi$ ), except if the sun’s position is at nadir. In the case of an isotropic diffuse irradiance field, without any direct irradiance component (closest approximated in the case of an optically thick cloud deck),  $\theta_i, \phi_i$  are omitted.
- If  $\omega_r = 2\pi$ ,  $\theta_r$  and  $\phi_r$  are omitted.

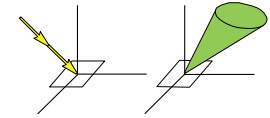
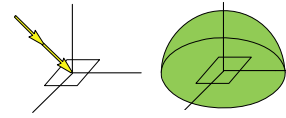
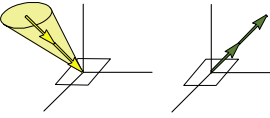
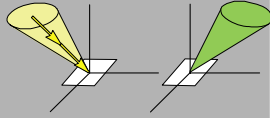
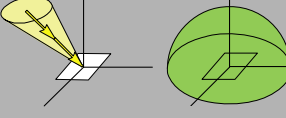
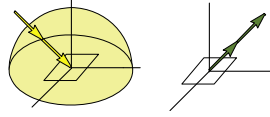
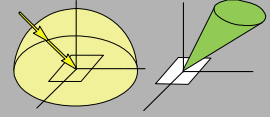
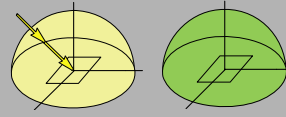
Finally, according to Nicodemus et al. (1977), the angular characteristics of the incoming radiance are named first in the term, followed by the angular characteristics of the reflected radiance. This leads to the attributes of radiance and reflectance quantities as illustrated in Table 2.

It should be noted that the nine standard reflectance terms defined by Nicodemus et al. (1977) “are applicable only to situations with uniform and isotropic radiation throughout the incident beam of radiation”. They then state that “If this is not true, then one must refer to the more general expressions”. This implies that any significant change to the nine reflectance concepts when the incident radiance is anisotropic lies in the mathematical expression used in their definition. Based on this implication, Martonchik et al. (2000) adapted the terminology and reflectance names to the remote sensing case, which involves direct and diffuse sky illumination. In the following, we give the mathematical description of the most commonly used quantities in remote sensing, thus the general expressions for non-isotropic incident radiation. When applicable, we simplify the expression for the special case of isotropic incident radiation. The nine possible combinations of beam geometries of the incident and reflected radiant fluxes are indicated as Cases 1 to 9, corresponding to the illustrations in Table 2.

2.2.1. The bidirectional reflectance distribution function (BRDF)—Case 1

The **bidirectional reflectance distribution function (BRDF)** describes the scattering of a parallel beam of incident light from one direction in the hemisphere into another direction in the hemisphere. The term BRDF was first used in the literature in the early 1960s (Nicodemus, 1965). Being expressed as the ratio of infinitesimal quantities, it cannot be directly measured (Nicodemus et al., 1977). The BRDF describes the intrinsic reflectance properties of a surface and

Table 2  
Relation of incoming and reflected radiance terminology used to describe reflectance quantities

Incoming/Reflected	Directional	Conical	Hemispherical
<i>Directional</i>	Bidirectional CASE 1 	Directional–conical CASE 2 	Directional–hemispherical CASE 3 
<i>Conical</i>	Conical–directional CASE 4 	Biconical CASE 5 	Conical–hemispherical CASE 6 
<i>Hemispherical</i>	Hemispherical–directional CASE 7 	Hemispherical–conical CASE 8 	Bihemispherical CASE 9 

The labeling with ‘Case’ corresponds to the nomenclature of Nicodemus et al. (1977). Grey fields correspond to measurable quantities (Cases 5, 8), the others (Cases 1–4, 6, 7, 9) denote conceptual quantities. Please refer to the text for the explanation on measurable and conceptual quantities.

thus facilitates the derivation of many other relevant quantities, e.g., conical and hemispherical quantities, by integration over corresponding finite solid angles.

The spectral BRDF can be expressed as

$$\begin{aligned} \text{BRDF}_\lambda &= f_r(\theta_i, \phi_i; \theta_r, \phi_r; \lambda) \\ &= \frac{dL_r(\theta_i, \phi_i; \theta_r, \phi_r; \lambda)}{dE_i(\theta_i, \phi_i; \lambda)} [\text{sr}^{-1}]. \end{aligned} \quad (1)$$

For reasons of clarity, we will omit the spectral dependence in the following. We therefore write for the BRDF

$$\text{BRDF} = f_r(\theta_i, \phi_i; \theta_r, \phi_r) = \frac{dL_r(\theta_i, \phi_i; \theta_r, \phi_r)}{dE_i(\theta_i, \phi_i)} [\text{sr}^{-1}]. \quad (2)$$

### 2.2.2. Reflectance factors—definition of Case 1 and Case 7

When reflectance properties of a surface are measured, the procedure usually follows the definition of a reflectance factor. The reflectance factor is the ratio of the radiant flux reflected by a sample surface to the radiant flux reflected into the identical beam geometry by an ideal (lossless) and diffuse (Lambertian) standard surface, irradiated under the same conditions as the sample surface. Following the different beam geometries of the incident and reflected radiant fluxes as mentioned above, we define the *bidirectional reflectance factor*, the *hemispherical–directional reflectance factor*, the *biconical reflectance factor*, and the *hemispherical–conical reflectance factor*.

The **bidirectional reflectance factor (BRF; Case 1)** is given by the ratio of the reflected radiant flux from the surface area  $dA$  to the reflected radiant flux from an ideal and diffuse surface of the same area  $dA$  under identical view geometry and single direction illumination:

$$\text{BRF} = R(\theta_i, \phi_i; \theta_r, \phi_r) = \frac{d\Phi_r(\theta_i, \phi_i; \theta_r, \phi_r)}{d\Phi_r^{\text{id}}(\theta_i, \phi_i)} \quad (3)$$

$$= \frac{\cos\theta_r \sin\theta_r dL_r(\theta_i, \phi_i; \theta_r, \phi_r) d\theta_r d\phi_r dA}{\cos\theta_r \sin\theta_r dL_r^{\text{id}}(\theta_i, \phi_i) d\theta_r d\phi_r dA} \quad (4)$$

$$= \frac{dE_i(\theta_i, \phi_i)}{dL_r^{\text{id}}(\theta_i, \phi_i)} \cdot \frac{dL_r(\theta_i, \phi_i; \theta_r, \phi_r)}{dE_i(\theta_i, \phi_i)} \quad (5)$$

$$= \frac{f_r(\theta_i, \phi_i, \theta_r, \phi_r)}{f_r^{\text{id}}(\theta_i, \phi_i)} = \pi f_r(\theta_i, \phi_i; \theta_r, \phi_r). \quad (6)$$

An ideal Lambertian surface reflects the same radiance in all view directions, and its BRDF is  $1/\pi$ . Thus, the BRF [unitless] of any surface can be expressed as its BRDF [ $\text{sr}^{-1}$ ] times  $\pi$  (Eq. (6)). For  $\Phi_r^{\text{id}}$  and  $L_r^{\text{id}}$ , we omit the view zenith and azimuth angles, because there is no angular dependence for the ideal Lambertian surface.

The concept of the **hemispherical–directional reflectance factor (HDRF; Case 7)** is similar to the definition of the BRF, but includes irradiance from the entire hemisphere. This makes

the quantity dependent on the actual, simulated or assumed atmospheric conditions and the reflectance of the surrounding terrain. This includes spectral effects introduced by the variation of the diffuse to direct irradiance ratio with wavelength (e.g., Strub et al., 2003).

$$\text{HDRF} = R(\theta_i, \phi_i, 2\pi; \theta_r, \phi_r) = \frac{d\Phi_r(\theta_i, \phi_i, 2\pi; \theta_r, \phi_r)}{d\Phi_r^{\text{id}}(\theta_i, \phi_i, 2\pi)} \quad (7)$$

$$= \frac{\cos\theta_r \sin\theta_r L_r(\theta_i, \phi_i, 2\pi; \theta_r, \phi_r) d\theta_r d\phi_r dA}{\cos\theta_r \sin\theta_r L_r^{\text{id}}(\theta_i, \phi_i, 2\pi) d\theta_r d\phi_r dA} \quad (8)$$

$$= \frac{L_r(\theta_i, \phi_i, 2\pi; \theta_r, \phi_r)}{L_r^{\text{id}}(\theta_i, \phi_i, 2\pi)} = \frac{\int_{2\pi} f_r(\theta_i, \phi_i; \theta_r, \phi_r) d\Phi_i(\theta_i, \phi_i)}{\int_{2\pi} (1/\pi) d\Phi_i(\theta_i, \phi_i)} \quad (9)$$

$$= \frac{\int_0^{2\pi} \int_0^{\pi/2} f_r(\theta_i, \phi_i; \theta_r, \phi_r) \cos\theta_i \sin\theta_i L_i(\theta_i, \phi_i) d\theta_i d\phi_i}{(1/\pi) \int_0^{2\pi} \int_0^{\pi/2} \cos\theta_i \sin\theta_i L_i(\theta_i, \phi_i) d\theta_i d\phi_i}. \quad (10)$$

If we divide  $L_i$  into a direct ( $E_{\text{dir}}$  with angles  $\theta_0, \phi_0$ ) and diffuse part, we may continue

$$= \frac{f_r(\theta_0, \phi_0; \theta_r, \phi_r) E_{\text{dir}}(\theta_0, \phi_0) + \int_0^{2\pi} \int_0^{\pi/2} f_r(\theta_i, \phi_i; \theta_r, \phi_r) \cos\theta_i \sin\theta_i L_i^{\text{diff}}(\theta_i, \phi_i) d\theta_i d\phi_i}{(1/\pi) (E_{\text{dir}}(\theta_0, \phi_0) + \int_0^{2\pi} \int_0^{\pi/2} \cos\theta_i \sin\theta_i L_i^{\text{diff}}(\theta_i, \phi_i) d\theta_i d\phi_i)} \quad (11)$$

then, if and only if  $L_i^{\text{diff}}$  is isotropic (i.e. independent of the angles), we may continue

$$= \frac{f_r(\theta_0, \phi_0; \theta_r, \phi_r) E_{\text{dir}}(\theta_0, \phi_0) + L_i^{\text{diff}} \int_0^{2\pi} \int_0^{\pi/2} f_r(\theta_i, \phi_i; \theta_r, \phi_r) \cos\theta_i \sin\theta_i d\theta_i d\phi_i}{(1/\pi) [E_{\text{dir}}(\theta_0, \phi_0) + L_i^{\text{diff}} \int_0^{2\pi} \int_0^{\pi/2} \cos\theta_i \sin\theta_i d\theta_i d\phi_i]} \quad (12)$$

$$= \pi f_r(\theta_0, \phi_0; \theta_r, \phi_r) \frac{(1/\pi) E_{\text{dir}}(\theta_0, \phi_0)}{(1/\pi) E_{\text{dir}}(\theta_0, \phi_0) + L_i^{\text{diff}}} + \int_0^{2\pi} \int_0^{\pi/2} f_r(\theta_i, \phi_i; \theta_r, \phi_r) \cos\theta_i \sin\theta_i d\theta_i d\phi_i \frac{L_i^{\text{diff}}}{(1/\pi) E_{\text{dir}}(\theta_0, \phi_0) + L_i^{\text{diff}}} \quad (13)$$

$$= R(\theta_0, \phi_0; \theta_r, \phi_r) d + R(2\pi; \theta_r, \phi_r) (1-d), \quad (14)$$

where  $d$  corresponds to the fractional amount of direct radiant flux (i.e.  $d \in [0, 1]$ ).

The **biconical reflectance factor (conical–conical reflectance factor, CCRF; Case 5)**, is defined as

$$\begin{aligned} \text{CCRF} &= R(\theta_i, \phi_i, \omega_i; \theta_r, \phi_r, \omega_r) \\ &= \frac{\int_{\omega_r} \int_{\omega_i} f_r(\theta_i, \phi_i; \theta_r, \phi_r) \cdot L_i(\theta_i, \phi_i) \cdot d\Omega_i \cdot d\Omega_r}{(\Omega_r/\pi) \cdot \int_{\omega_i} L_i(\theta_i, \phi_i) \cdot d\Omega_i}, \end{aligned} \quad (15)$$

where  $\Omega = [d\Omega = [\cos\theta d\omega = ] [\cos\theta \sin\theta d\theta d\phi]$  is the projected solid angle of the cone.

Formally, the CCRF can be seen as the most general quantity, because its expression contains all other cases as special ones: for  $\omega=0$  the integral collapses and we obtain the directional

case, and for  $\omega=2\pi$  we obtain the hemispherical case. However, the BRF and BRDF remain the most fundamental and desired quantities because they are the only quantities not integrated over a range of angles.

For large IFOV sensor measurements performed under ambient sky illumination, the assumption of a zero interval of the solid angle for the measured reflected radiance beam does not hold true. The resulting quantity most precisely could be described as **hemispherical–conical reflectance factor (HCRF; Case 8)**, obtained from Eq. (15) by setting  $\omega_i=2\pi$ :

$$\begin{aligned} \text{HCRF} &= R(\theta_i, \phi_i, 2\pi; \theta_r, \phi_r, \omega_r) \\ &= \frac{\int_{\omega_r} \int_{2\pi} f_r(\theta_i, \phi_i; \theta_r, \phi_r) \cdot L_i(\theta_i, \phi_i) \cdot d\Omega_i \cdot d\Omega_r}{(\Omega_r/\pi) \cdot \int_{2\pi} L_i(\theta_i, \phi_i) \cdot d\Omega_i}. \end{aligned} \quad (16)$$

### 2.2.3. Reflectance—Case 3 and Case 9

In the following, we describe the hemispherical reflectance as a function of different irradiance scenarios including (i) the special condition of pure direct irradiance, (ii) common Earth irradiance, composed of diffuse and direct components, and (iii) pure diffuse irradiance.

The **directional–hemispherical reflectance (DHR; Case 3)** corresponds to pure direct illumination (reported as black-sky albedo in the MODIS product suite (Lucht et al., 2000)). It is the ratio of the radiant flux for light reflected by a unit surface area into the view hemisphere to the illumination radiant flux, when the surface is illuminated with a parallel beam of light from a single direction.

$$\begin{aligned} \text{DHR} &= \rho(\theta_i, \phi_i, 2\pi) = \frac{d\Phi_r(\theta_i, \phi_i, 2\pi)}{d\Phi_i(\theta_i, \phi_i)} \\ &= \frac{dA \int_0^{2\pi} \int_0^{\pi/2} dL_r(\theta_i, \phi_i; \theta_r, \phi_r) \cos\theta_r \sin\theta_r d\theta_r d\phi_r}{d\Phi_i(\theta_i, \phi_i)} \end{aligned} \quad (17)$$

$$= \frac{d\Phi_i(\theta_i, \phi_i) \int_0^{2\pi} \int_0^{\pi/2} f_r(\theta_i, \phi_i; \theta_r, \phi_r) \cos\theta_r \sin\theta_r d\theta_r d\phi_r}{d\Phi_i(\theta_i, \phi_i)} \quad (18)$$

$$= \int_0^{2\pi} \int_0^{\pi/2} f_r(\theta_i, \phi_i; \theta_r, \phi_r) \cos\theta_r \sin\theta_r d\theta_r d\phi_r. \quad (19)$$

The **bihemispherical reflectance (BHR; Case 9)**, generally called albedo, is the ratio of the radiant flux reflected from a unit surface area into the whole hemisphere to the incident radiant flux of hemispherical angular extent.

$$\text{BHR} = \rho(\theta_i, \phi_i, 2\pi; 2\pi) = \frac{d\Phi_r(\theta_i, \phi_i, 2\pi; 2\pi)}{d\Phi_i(\theta_i, \phi_i, 2\pi)} \quad (20)$$

$$= \frac{dA \int_0^{2\pi} \int_0^{\pi/2} dL_r(\theta_i, \phi_i, 2\pi; \theta_r, \phi_r) \cos\theta_r \sin\theta_r d\theta_r d\phi_r}{dA \int_0^{2\pi} \int_0^{\pi/2} dL_i(\theta_i, \phi_i) \cos\theta_i \sin\theta_i d\theta_i d\phi_i} \quad (21)$$

$$= \frac{\int_0^{2\pi} \int_0^{\pi/2} \int_0^{2\pi} \int_0^{\pi/2} f_r(\theta_i, \phi_i; \theta_r, \phi_r) \cos\theta_r \sin\theta_r d\theta_r d\phi_r L_i(\theta_i, \phi_i) \cos\theta_i \sin\theta_i d\theta_i d\phi_i}{\int_0^{2\pi} \int_0^{\pi/2} L_i(\theta_i, \phi_i) \cos\theta_i \sin\theta_i d\theta_i d\phi_i} \quad (22)$$

$$= \frac{\int_0^{2\pi} \int_0^{\pi/2} \rho(\theta_i, \phi_i; 2\pi) L_i(\theta_i, \phi_i) \cos\theta_i \sin\theta_i d\theta_i d\phi_i}{\int_0^{2\pi} \int_0^{\pi/2} L_i(\theta_i, \phi_i) \cos\theta_i \sin\theta_i d\theta_i d\phi_i}. \quad (23)$$

If as before we divide  $L_i$  into a direct ( $E_{\text{dir}}$  with angles  $\theta_0, \phi_0$ ) and diffuse part, and assume that  $L_i^{\text{diff}}$  is isotropic we can write

$$= \frac{\rho(\theta_0, \phi_0; 2\pi) E_{\text{dir}}(\theta_0, \phi_0) + \pi L_i^{\text{diff}}(1/\pi) \int_0^{2\pi} \int_0^{\pi/2} \rho(\theta_i, \phi_i; 2\pi) \cos\theta_i \sin\theta_i d\theta_i d\phi_i}{E_{\text{dir}}(\theta_0, \phi_0) + \pi L_i^{\text{diff}}} \quad (24)$$

$$= \rho(\theta_0, \phi_0; 2\pi) d + \rho(2\pi; 2\pi)(1-d), \quad (25)$$

where  $d$  again corresponds to the fractional amount of direct radiant flux.

For the special case of pure diffuse isotropic incident radiation, a situation that may be most closely approximated in the field by a thick cloud or aerosol layer, the resulting BHR (reported as white-sky albedo in the MODIS product suite (Lucht et al., 2000)) can be described as follows

$$\begin{aligned} \text{BHR} &= \rho(2\pi; 2\pi) \\ &= \frac{1}{\pi} \int_0^{2\pi} \int_0^{\pi/2} \rho(\theta_i, \phi_i; 2\pi) \cos\theta_i \sin\theta_i d\theta_i d\phi_i. \end{aligned} \quad (26)$$

Under ambient illumination conditions, the albedo is influenced by the combined diffuse and direct irradiance. To obtain an approximation of the albedo for ambient illumination conditions (also reported as blue-sky albedo in the MODIS product suite), it is suggested to linearly combine the BHR for isotropic diffuse illumination conditions and the DHR (see Eq. (25)), corresponding to the actual ratio of diffuse to direct illumination (Lewis & Barnsley, 1994; Lucht et al., 2000). The diffuse component then can be expressed as a function of wavelength, optical depth, aerosol type, and terrain contribution. The underlying assumption of an isotropic diffuse illumination may lead to significant uncertainties due to ignoring the actual distribution of the incoming diffuse radiation.

All abovementioned albedo values, with the exception of the BHR for pure diffuse illumination conditions, depend on the actual illumination angle of the direct component. Thus, it is highly recommended to include the solar geometry when describing albedo quantities.

### 2.3. Examples for measurable quantities and derived products

In Table 2, we present the typical incoming and reflected beam geometries in relation to the individual reflectance cases discussed above. From a strict physical point of view, the most common measurement setup of satellites, airborne and field instruments corresponds to the hemispherical–conical configuration (Case 8) (e.g., MERIS/ENVISAT, Analytical Spectral Devices FieldSpec). In general, space-based instruments with a spatial resolution of about 1 km have a IFOV with a full cone

angle of approximately  $0.1^\circ$  (e.g., MISR, MODIS, AVHRR). If the HDRF is constant over the full cone angle of the instrument IFOV, then the HCRF numerically equals the HDRF. Based on this assumption, the reflectance products from these instruments are often being referred to as HDRF and BRDF instead of HCRF and DCRF, without further correction for the conical observation angle. Field instruments like PARABOLA or ASG with a IFOV full cone angle of about  $4^\circ$  to  $5^\circ$ , the significance of the surface directional reflectance variability needs to be investigated. As long as the variability is unknown, these measurements should be reported as HCRF.

Albedometer measurements approximate the bihemispherical configuration (Case 9) (e.g., Kipp & Zonen, 2000). Finally, a typical laboratory setup corresponds to the biconical configuration (Case 5), where a light source illuminates a target that is measured using a non-imaging spectroradiometer (e.g., EGO (Koechler et al., 1994), LAGOS (Dangel et al., 2005), or ASG (Painter et al., 2003) used in the laboratory). For a perfectly collimated light source (find a detailed description of the problem in Dangel et al., 2005), these measurements approximate the directional–conical quantity.

The derivation of different at-surface reflectance quantities from measurements requires a sophisticated processing, as implemented, for example, in the MISR scheme. The integration of the at-surface HDRF (Case 7) over the viewing hemisphere results in the BHR (Case 9). Using a modeling approach to eliminate the diffuse illumination effects of the HDRFs (Lyapustin & Privette, 1999; Martonchik, 1994; Martonchik et al., 1998), BRDF data are derived (Case 1). The hemispherical integration of the BRDFs over the viewing hemisphere yields DHR data. MISR albedo products include BHR (blue-sky albedo) and DHR (black-sky albedo), whereas MODIS albedo products include BHR for isotropic diffuse illumination conditions (white-sky albedo) and DHR (black-sky albedo).

These derivations of conceptual reflectance quantities from measured reflectance data include the application of a BRDF model. Thus, derived conceptual quantities depend not only on the sampling scheme, availability and accuracy of measured data, but also on the properties and accuracy of the model.

### 3. Current usage of reflectance terminology

The multi-angular measurement configuration of MISR facilitates the derivation of different reflectance products using consistent terminology. For many other satellite and airborne systems, the user community is faced with products simply called ‘surface reflectance’ or ‘apparent surface reflectance’. Without detailed information on the preprocessing of the observed data and beam geometries of the resulting reflectance products, these data are subject to misinterpretation and greater uncertainty.

We consider a physically consistent expression of reflectance quantities as a prerequisite in peer-reviewed literature. The presented concept of reflectance terminology is available to the user community, yet the literature contains prolific ambiguous and erroneous use of terminology for measured and derived

reflectance quantities. Below we present a selection of articles as exemplary for a wide range of publications indicating the breadth of the challenge.

#### 3.1. Ambiguous usage

We identified a widely spread ambiguous use of the terms ‘reflectance’, ‘surface reflectance’, and ‘albedo’, as these do not accurately specify measured or derived physical quantities. This is of particular importance if details on data acquisition and atmospheric correction are missing.

Amongst many others, Roberts et al. (1993) use the ambiguous term ‘reflectance’ when referring to field measurements with a spectrometer and empirically corrected imaging spectrometer data, and once mention that ‘bidirectional reflectance’ is measured in the field. All measurements discussed in the above reference are *hemispherical–conical reflectance factors* due to the contribution of direct and diffuse components to the irradiance field.

Most satellite sensor products are reported as ‘surface reflectance’ (e.g., MODIS MOD09 (Vermeulen & Vermeulen, 1999), ETM+ data processed after Liang et al. (2001)). When data of different sensors are combined or compared, the physics behind these products must be more carefully examined to prevent ambiguous results in future studies (e.g., Fang et al., 2004).

The ambiguous use of the terms ‘reflectance’ and ‘albedo’ is especially critical when reference databases that contain different physical quantities are compiled. There is a high probability that the presented numbers will be applied without analyzing uncertainties introduced by their different definitions, especially when potential users are not familiar with remote sensing data and processing (Breuer et al., 2003).

#### 3.2. Erroneous usage

Secondly, the terms ‘directional’, ‘bidirectional’, and ‘BRDF’ are widely used when referring to measured reflectance quantities. As explained above, these quantities cannot be measured, but are approximated by measurements and subsequent atmospheric correction and angular modeling. Even applying an atmospheric correction algorithm to measured radiance data does not per se result in bidirectional reflectance products, as different algorithms account for different parts of the atmospheric contribution. We therefore briefly discuss the different atmospheric contributions, as described in Lee and Kaufman (1986).

The radiance of light reflected from the Earth and the atmosphere ( $L_r$ ) is composed of three components:

$$L_r = L_r^{\text{atm}} + L_r^{\text{dir}} + L_r^{\text{diff}}, \quad (27)$$

where  $L_r^{\text{atm}}$  is the radiance of light scattered from the direct sun beam into the sensor’s field of view (FOV) without being reflected by the surface, and is often called atmospheric path radiance.  $L_r^{\text{dir}}$  is the radiance of sunlight transmitted directly through the atmosphere, then reflected by the surface, and then

directly transmitted through the atmosphere. Diffuse radiance  $L_r^{\text{diff}}$  consists of three components:

$$L_r^{\text{diff}} = L_r^{\text{diff1}} + L_r^{\text{diff2}} + L_r^{\text{diff3}}, \quad (28)$$

whereas  $L_r^{\text{diff1}}$  is the contribution of diffuse light scattered by the atmosphere before reaching the surface and then directly transmitted to the sensor,  $L_r^{\text{diff2}}$  is the contribution of diffuse light transmitted directly to the surface and then scattered by the atmosphere toward a sensor after being reflected by the surface, and  $L_r^{\text{diff3}}$  is the contribution of light scattered by the atmosphere both before and after being reflected from the surface. This formulation is applicable for a uniform surface, whereas for high spatial resolution remote sensing data, the adjacency effect must also be corrected. This description shows that for the derivation of bidirectional reflectance factors, the atmospheric path radiance and all three diffuse components must be subtracted from the reflected radiance, whereas many atmospheric correction algorithms account only for the path radiance  $L_r^{\text{atm}}$ , and diffusely transmitted contributions to the sensor (i.e.,  $L_r^{\text{diff2}}$  and  $L_r^{\text{diff3}}$ ).

For measurements close to the ground surface, the atmospheric path radiance ( $L_r^{\text{atm}}$ ),  $L_r^{\text{diff2}}$ , and  $L_r^{\text{diff3}}$  are essentially all zero. Thus, these measurements already represent surface-leaving radiance. Bidirectional reflectance properties can be derived from ground reflectance measurements by deducing the contribution of the hemispherical diffuse irradiance from the total reflectance signal (e.g., Lyapustin & Privette, 1999; Martonchik, 1994). Most publications report uncorrected surface reflectance (Lyapustin & Privette, 1999) but refer to them as ‘BRDF’ or ‘BRF’, instead of hemispherical–conical reflectance quantities. Nolin and Liang (2000) indicate that “[e]mpirically, the BRDF of a surface is determined by discrete sampling of the angular radiance at finite solid angles.” The important correction here is that the BRDF is *approximated* but not determined by discrete sampling of the angular radiance at finite solid angles.

Erroneous terminology is observed for measurements of most multiangular field instruments, including PARABOLA (Deering et al., 1990), FIGOS (Sandmeier & Itten, 1999), and other multiangular measurement setups (e.g., Chopping, 2000; Susaki et al., 2004). Some authors acknowledge that BRDF or BRF cannot be measured, but—based on unphysical statements—still refer to their measurements as bidirectional. Others suggest technical solutions in the field (e.g. measuring the contribution of the diffuse irradiance by shading of the direct sunlight using a screen (Peltoniemi et al., 2005)). The measured reflectance under diffuse conditions is then deduced from the total reflectance. As the strong forward scattering phase function of aerosols dictates that most of the diffuse irradiance follows a downward path close to the original solar path (Lyapustin & Privette, 1999), a significant part of the diffuse contribution is shaded by the screen as well. The shading geometry itself indicates that a conical irradiance is left after deducing the diffuse component outside the shading screen. Further, the remaining conical irradiance is still composed of a diffuse and direct part, and resulting reflectance quantities are therefore biconical. This may result in spectral

distortions of the derived biconical reflectance distribution function compared to the surface BRDF, and therefore is still solely an approximation of the BRDF.

For airborne and spaceborne sensors, perturbations to the downwelling and upwelling radiation streams contribute to the overall observed reflectance. The wide variety of atmospheric correction algorithms applied to airborne sensor data accounts for different combinations of atmospheric contributions deduced from the at-sensor radiance to calculate the so-called ‘at-surface reflectances’. One example is the ATCOR atmospheric processing chain (Richter & Schlapfer, 2002), where at-sensor radiance is corrected for the path radiance and adjacency effect, but not for the hemispherical irradiance. The resulting ambiguously named ‘surface reflectance’ thus corresponds to HDRF data. The multiangular data products of air- and spaceborne POLDER are currently reported as ‘BRDF’ data, while they lack a full aerosol correction (e.g., Bacour & Breon, 2005; Grant et al., 2003). On the other hand, the atmospheric correction applied to AirMISR data delivers the full suite of reflectance products (HDRF, BRF, BHR, and DHR) as available for its spaceborne counterpart MISR.

Radiative transfer models typically allow the incorporation of a pure direct, pure diffuse, or combined direct and diffuse irradiance. Thus, depending on the purpose of modeled reflectance, BRF data (only direct irradiance), or HDRF data (pure diffuse or a combination of direct and diffuse irradiance) can be modeled. When running the models over a wide wavelength range (e.g., for the analysis of imaging spectrometer data), the diffuse to direct irradiance ratio must be wavelength dependent, due to spectral nature of Mie and Rayleigh scattering. Current vegetation studies often assume this ratio to be wavelength independent (e.g., Atzberger, 2004; Koetz et al., 2004), and thus modeled reflectances are expected to be spectrally distorted compared to measured data.

Even though the terms ‘bidirectional’ and ‘BRDF’ are part of the established nomenclature for the reflectance products of many in situ, air- and spaceborne sensors, while still including the hemispherical irradiance contribution, this does not change the physical inadequacy of this terminology and the consequent questionable interpretation of the respective reflectance products. As the terms ‘surface reflectance’ and ‘at-surface reflectance’ do not allow for the determination of the irradiance conditions of the data product, we advise to follow a more precise terminology as given above, using HDRF, HCRF, BRF, DCRF, DHR, and BHR. For general study and data descriptions we further suggest using more appropriate terms, such as ‘reflectance anisotropy’ or ‘multiangular’, instead of the commonly applied terms ‘BRDF’, ‘directional’, and ‘bidirectional’, while preserving the latter for the true conceptual physical quantities.

#### 4. Quantitative comparison of reflectance quantities

The following case studies highlight differences of the described reflectance quantities using (i) MISR data products for several selected biome types, (ii) model simulations for a vegetation canopy, and (iii) model simulations for snow cover.

Table 3  
Overview of MISR data selected for the analysis of the land surface reflectance products

Site	Acquisition date in 2001	SZ [°]	AOD	IGBP biome type
Howland, Maine, USA	07/21	27.7	0.10	Mixed forests, deciduous broadleaf forests, evergreen needleleaf forests
Railroad Valley, Nevada, USA	08/17	28.4	0.10	Open shrublands, grasslands, woody savannas
Mongu, Zambia	07/11	44.6	0.05	Savannas, cropland/natural vegetation mosaic, woody savannas, grasslands
Banizoumbou, Niger	10/04 12/23	24.1 41.4	0.31 0.11	Open shrublands, grasslands, savannas
Hombori, Mali	07/05	19.6	0.36	Open shrublands, barren or sparsely vegetated, grasslands
Avignon, France	07/12 08/29	25.2 36.9	0.07 0.19	Croplands, mixed forest, water bodies
Bordeaux, France	05/30 07/01	24.5 24.0	0.24 0.12	Evergreen needleleaf forests, croplands, cropland/natural vegetation mosaic, woody savannas, mixed forests

SZ corresponds to the scene-averaged solar zenith angle, whereas AOD is the scene-averaged aerosol optical depth at 558 nm over all valid pixels.

The differences of hemispherical versus directional reflectance and reflectance factors (i.e., BHR (Case 9) versus DHR (Case 3) and HDRF (Case 7) versus BRF (Case 1)) are computed for the visible to shortwave infrared wavelength range, and different ratios of direct to diffuse illumination conditions.

The analysis of MISR data highlights differences in reflectance quantities resulting from data, algorithm, and model uncertainties, as well as different aerosol optical depth (AOD). Thus, it reveals expected differences in real satellite data products, whereas the two simulation studies emphasize the general features of reflectance quantities for vegetation and snow.

#### 4.1. Analysis of MISR surface reflectance data products

##### 4.1.1. Methods and selected data sets

Various land surface reflectance products are available from the MISR sensor, retrieved from observations of nine cameras (center view directions of  $0^\circ$ ,  $\pm 26.1^\circ$ ,  $\pm 45.6^\circ$ ,  $\pm 60.0^\circ$ , and  $\pm 70.5^\circ$ ) in four spectral bands (446, 558, 672, and 867 nm) (Diner et al., 1999). The top-of-atmosphere MISR radiances are atmospherically corrected to produce HDRF and BHR data, surface reflectance properties as would be measured at ground level but at the MISR spatial resolution of 1.1 km. The HDRF and BHR are then corrected for diffuse illumination effects, and fitted to a three-parameter empirical BRDF model, resulting in the BRF and DHR (Martonchik et al., 1998).

We statistically analyzed the differences of directional and hemispherical reflectance products, namely DHR versus BHR and BRF versus HDRF, by their mean values, mean absolute and relative difference, and correlation.

The ratio of diffuse to direct illumination is an increasing function of the atmospheric optical depth. The AOD decreases with wavelength due mainly to the decreasing influence of Rayleigh scattering and, to a lesser extent in most cases, aerosols. For example, at 1000 hPa, Rayleigh scattering contributes 0.236, 0.094, 0.044, and 0.016 to the atmospheric optical depth in the blue, green, red, and near-infrared band, respectively (Russell et al., 1993). Thus, we expected the largest product difference in short wavelength ranges, with a maximum in the blue band.

We selected 10 2001 MISR data sets that span different biome types (Friedl et al., 2002) and correspond to data product version 12 (Lewicki et al., 2003). Three sites were covered twice under different atmospheric conditions and sun zenith angles (Table 3). The reliability of the land surface reflectance values depends on the AOD magnitude, as the contribution of the surface to the overall signal decreases with increasing AOD. Therefore, pixels with a large optical depth in the green spectral band (greater 0.5) were excluded from calculations. All

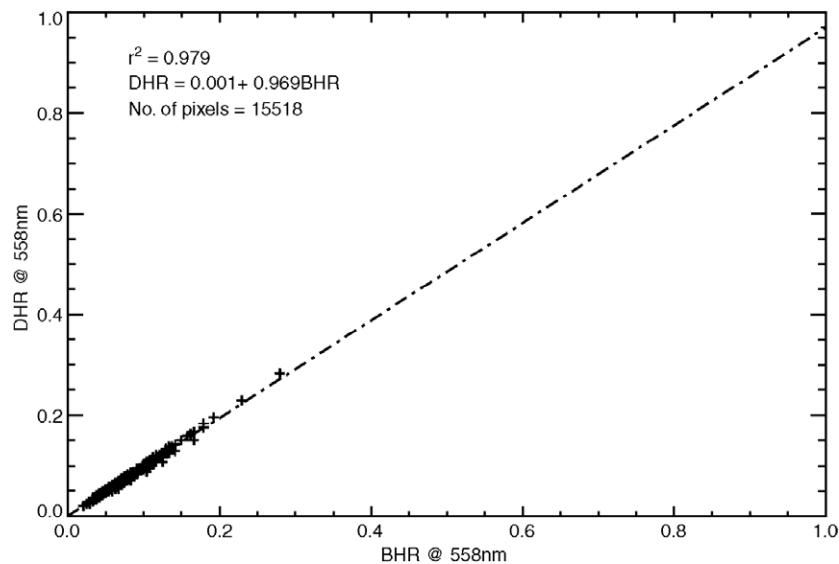


Fig. 1. Relation between BHR and DHR exemplified by the green spectral band of the Howland scene.

Table 4  
Comparison of BHR and DHR values for the selected MISR scenes

Site	SZ [°]	AOD, 558 nm	Mean BHR/Mean((BHR – DHR)/BHR) [%]			
			446 nm, blue	558 nm, green	672 nm, red	867 nm, NIR
Howland	27.7	0.10	0.031/2.1	0.053/1.5	0.028/1.1	0.318/0.7
Railroad Valley	28.4	0.10	0.095/1.7	0.137/1.3	0.170/0.9	0.238/0.7
Mongu	44.6	0.05	0.046/0.5	0.078/0.3	0.094/0.3	0.246/0.6
Banizoumbou	24.1	0.31	0.060/1.2	0.126/1.5	0.176/1.4	0.357/1.3
	41.4	0.11	0.084/0.5	0.160/0.5	0.261/0.6	0.376/0.6
Hombori	19.6	0.36	0.108/5.1	0.232/2.5	0.349/1.6	0.412/1.2
Avignon	25.2	0.07	0.045/2.0	0.075/1.4	0.069/0.9	0.307/0.8
	36.9	0.19	0.050/0.9	0.081/0.9	0.079/0.7	0.286/0.8
Bordeaux	24.5	0.24	0.059/1.5	0.097/2.0	0.087/1.4	0.320/1.2
	24.0	0.12	0.048/1.8	0.078/1.5	0.073/1.0	0.304/0.9

The aerosol optical depth at 558 nm, averaged over all analyzed pixels, is indicated, as well as BHR mean values and BHR to DHR differences, in relation to the BHR.

quantities called ‘scene-averaged’ rely on this exclusion. Additionally, the products, ‘HDRF uncertainty averaged over all cameras’ and the ‘relative BHR uncertainty’ were analyzed. We assume that these uncertainties also apply to the BRF and DHR products ([http://eosweb.larc.nasa.gov/PRODOCS/misr/Quality\\_Summaries/L2\\_AS\\_Products\\_20030125.html](http://eosweb.larc.nasa.gov/PRODOCS/misr/Quality_Summaries/L2_AS_Products_20030125.html)).

4.1.2. Differences between BHR (Case 9) and DHR (Case 3)

MISR BHR and DHR products are highly correlated in all spectral bands and scenes ( $0.84 < r^2 < 1.0$ ) (Fig. 1). The relative scene-averaged difference between BHR and DHR reaches a maximum of 2.7% of the BHR value (with the exception of the

blue band of the Hombori scene reaching 5.1%) for all four spectral bands (Table 4). The lowest scene-averaged relative BHR uncertainty is 5.6% for the NIR spectral band of the Avignon (07/12) scene, whereas relative BHR uncertainty can reach 20% and higher, with a maximum of 88% for the blue spectral band of the Banizoumbou (10/04) scene. Thus, differences between BHR and DHR are very small compared to actual product uncertainties.

We expect a trend of decreasing differences between BHR and DHR with increasing wavelength, wherein the blue band reflectances should show the biggest relative differences. This is confirmed by results of five scenes, whereas for the other five cases, differences reach the same or even higher values in at least one of the other bands. Note that the differences are a combination of effects caused by the AOD, scattering effects of the surroundings, and the sensitivity of the BRDF to the angle of the incident radiance with wavelength. Thus, if the surface shows almost Lambertian reflectance properties in the blue spectral region, but a much higher anisotropy in the NIR spectral region, then the HDRF approximates the BRF (see Eq. (10)) for the blue spectral region, whereas the difference between the two quantities can be much bigger in the NIR spectral region.

Differences between the BHR and DHR product can be related to the actual aerosol optical depth in the green spectral band (Fig. 2). This relationship has  $r^2=0.29$  for the blue band and increases with increasing wavelengths, with a maximum for the NIR region ( $r^2=0.79$ ). A strong negative correlation is found between the relative BHR to DHR difference and the solar zenith angle ( $r^2=0.51, 0.88, 0.82, 0.51$  for the blue, green, red, NIR band, respectively) (Fig. 3). The biggest difference between BHR and DHR occurs around solar noon.

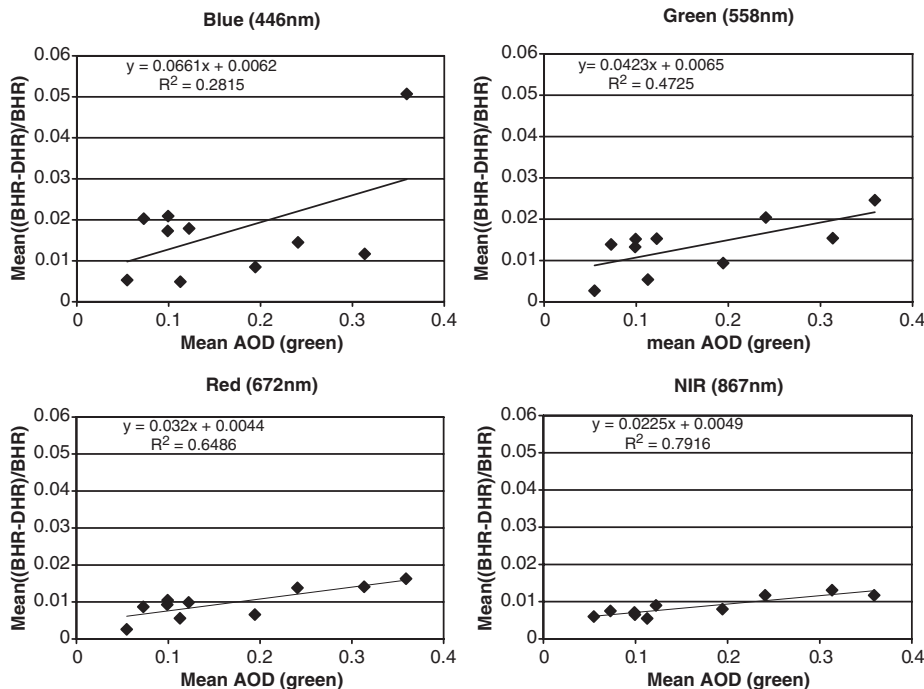


Fig. 2. Relation of relative BHR\_DHR differences for all MISR spectral bands with mean aerosol optical depth in the green spectral band. Data points correspond to analyzed scenes.

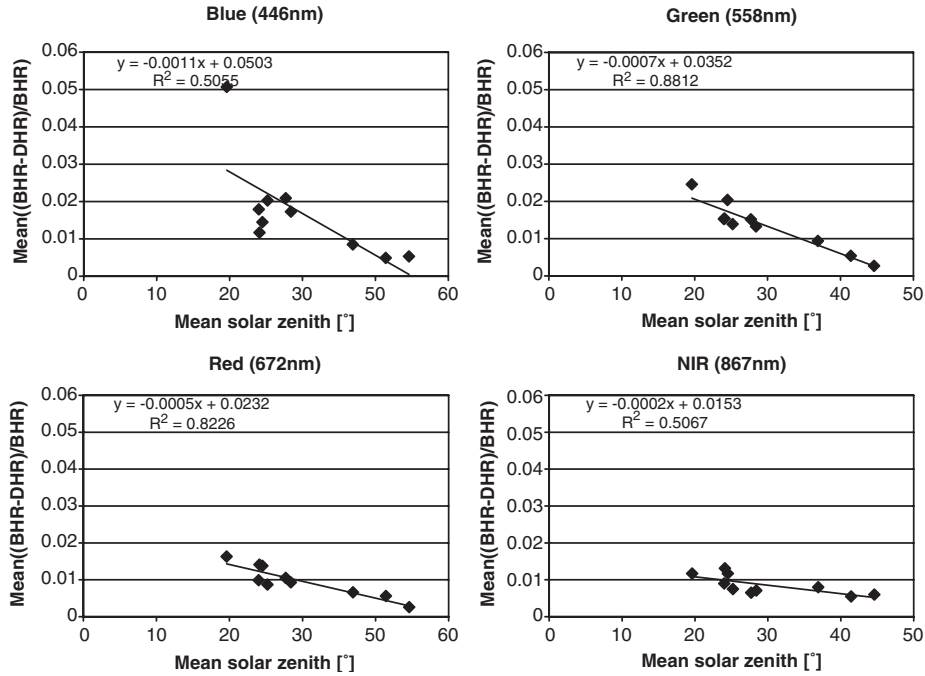


Fig. 3. Relation of relative BHR-DHR differences in all four MISR spectral bands with mean solar zenith angle. Data points correspond analyzed scenes.

4.1.3. Differences between HDRF (Case 7) and BRF (Case 1)

HDRF and BRF are highly correlated ( $r^2 > 0.98$ ) throughout most spectral bands and view angles of all scenes (Fig. 4). Compared to the quantities integrated over the view hemisphere, the relative differences of the single view angle reflectances are larger and reach up to 14% of the HDRF value. Regarding the viewing direction, there is a significant trend of decreased HDRF–BRF differences for the afterward looking cameras, with the Ba camera (view zenith 45.6°) showing the smallest differences for most scenes and spectral bands. Only a weak correlation ( $r^2 = 0.27$ ) is found between the green spectral band AOD and the relative HDRF–BRF difference averaged over all spectral bands and cameras for each scene (Fig. 5).

4.2. Vegetation canopy reflectance simulations using the RPV model

4.2.1. Methods and data

Using the PARABOLA instrument (Deering & Leone, 1986), black spruce forest HCRF data were observed at eight solar zenith angles (35.1°, 40.2°, 45.2°, 50.2°, 55.0°, 59.5°, 65.0°, 70.0°) (Deering et al., 1995). As this study is based on a past field measurements, we have to assume that the surface directional reflectance variability within the PARABOLA IFOV can be neglected and subsequently report measurements as HDRF. After applying a simple HDRF to BRF atmospheric correction (Tanre et al., 1983), data of the red spectral band

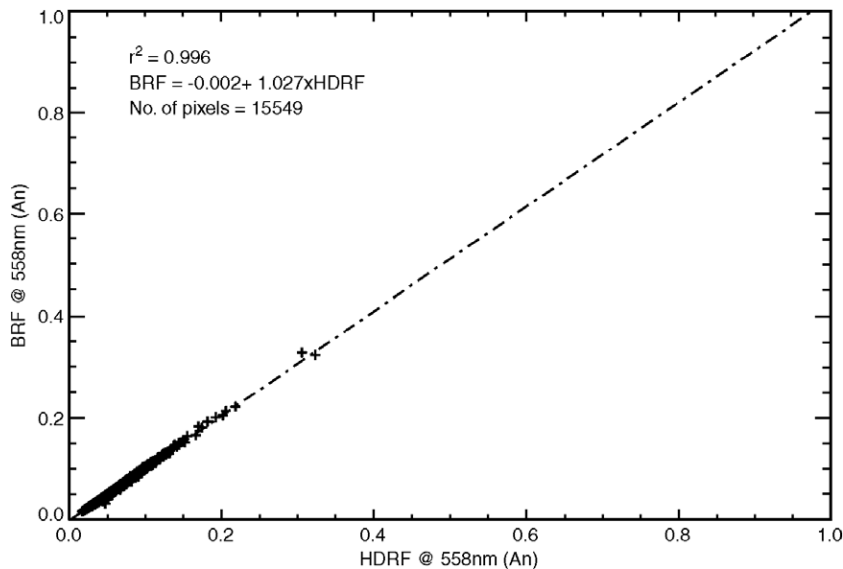


Fig. 4. Relation between HDRF and BRF exemplified by the green spectral band of the MISR nadir looking camera (An) of the Howland scene.

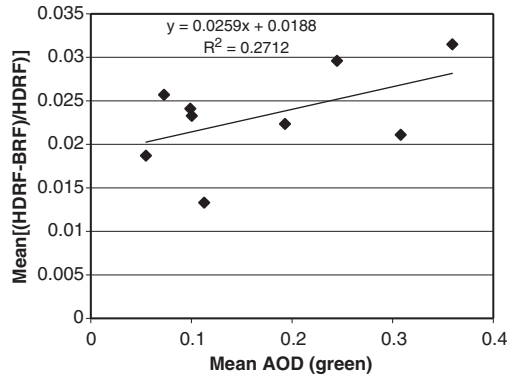


Fig. 5. Correlation between mean aerosol optical depth in the green spectral band and the relative HDRF-BRF difference, averaged over each scene, all spectral bands and cameras of the MISR sensor.

(650–670 nm) were fitted to the parametric Rahman–Pinty–Verstraete (RPV) model (Engelsen et al., 1996; Rahman et al., 1993). We used resulting fit parameters and the RPV model to simulate different reflectance quantities of a black spruce canopy under various illumination conditions. The model was run for a solar zenith angle of 30° and increments of direct ( $d$ ) and diffuse ( $1-d$ ) irradiance of  $d=1.0, 0.8, 0.6, 0.4, 0.2, 0.0$ . The irradiance scenario  $d=1.0$  corresponds to BRF or DHR, whereas all others represent HDRF or BHR.

4.2.2. Results

As expected for a vegetation canopy, backscattering is the dominating reflectance feature for the black spruce BRF data, with a pronounced hot spot at a view zenith of 30° (Figs. 6 and 7). Adding an isotropic diffuse irradiance component results in

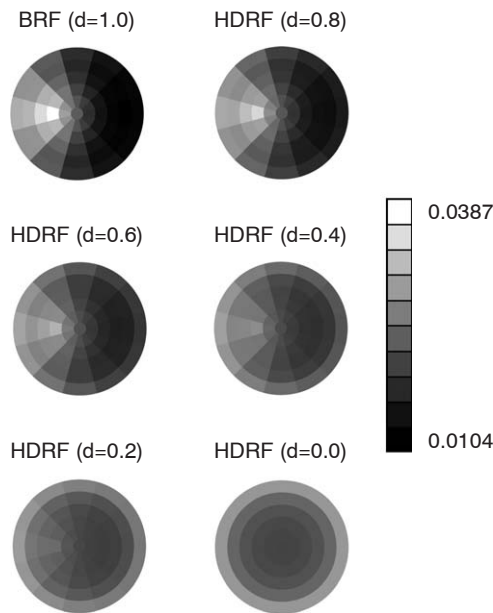


Fig. 6. Reflectance factors of a black spruce forest canopy at 650–670 nm as a function of view angle. The direct illumination, at 30° zenith, is from the left. The six plots illustrate the influence of the relative amount of direct illumination. The top left image corresponds to pure direct irradiation, thus to BRF data, all others to HDRF data (from  $d=0.8$  to  $d=0$ ). The bottom right image corresponds to totally diffuse illumination ( $d=0$ ).

HDRF data. With decreasing direct irradiance, the anisotropy is smoothed. Finally, the hot spot disappears for a scenario based on diffuse irradiance only. Concentrating on nadir view data, the relative difference between the bidirectional and the hemispherical–directional reflectance factor can be significant, especially for illumination zenith angles around solar noon, approaching the hot spot configuration (Fig. 7). The general pattern of increasing differences between HDRF and BRF with decreasing solar zenith angle agree qualitatively with the empirical results of the MISR data analysis (Fig. 3). Even though absolute differences between single BRF and HDRF data are numerically small for the selected wavelength range and certain geometries, it becomes obvious that BRDF functions can be strongly distorted when derived from model fits based on HDRF instead of BRF data.

Also as expected for vegetation, the DHR increases with increasing illumination zenith (Kimes, 1983), whereas the BHR

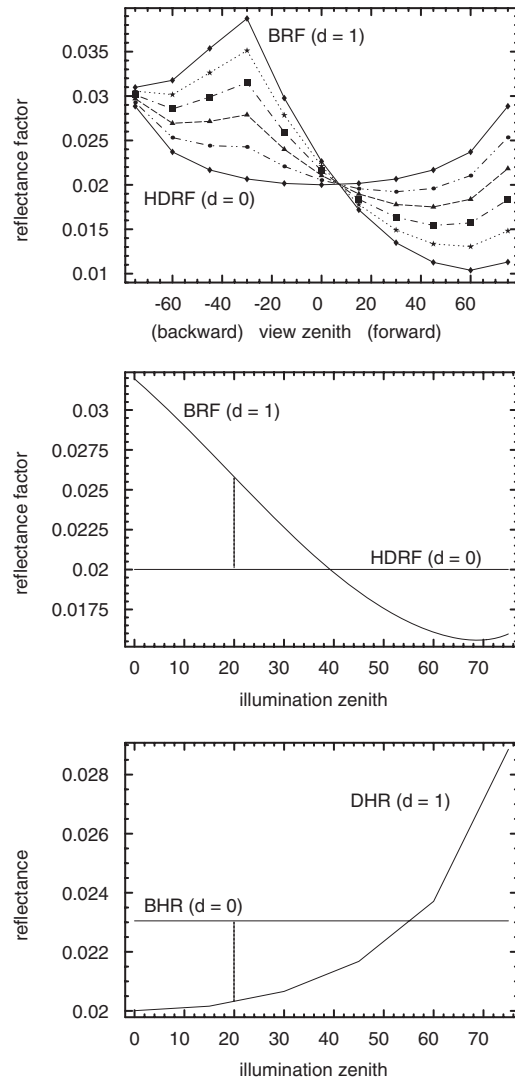


Fig. 7. Simulated BRF ( $d=1.0$ ) and HDRF ( $d=0.8$  to  $d=0.0$ ) data for a black spruce canopy in the solar principal plane (top); BRF ( $d=1.0$ ) and HDRF (isotropic diffuse illumination conditions ( $d=0.0$ )) at nadir view geometry (centre); DHR ( $d=1.0$ ) and BHR (isotropic diffuse illumination ( $d=0.0$ )) (bottom).

for isotropic diffuse irradiance conditions (white-sky albedo) is independent of the illumination angle (Fig. 7). According to Eq. (25), the albedo for ambient sky conditions (blue-sky albedo) can be approximated by a combination of DHR and BHR for isotropic incident radiation (white-sky albedo). For a given illumination zenith angle (e.g., 20° (Fig. 8)) the approximated BHR for ambient sky conditions then lies on a vertical line between the DHR and BHR for isotropic incident radiation which depend on the actual ratio of diffuse to direct irradiance.

### 4.3. Snow reflectance simulations

#### 4.3.1. Methods and data

This case study presents results from snow directional reflectance simulations, coupling single-scattering parameters and the discrete-ordinates multiple scattering model DISORT (Stamnes et al., 1988). The single-scattering parameters used in

the model are the single-scattering albedo, extinction efficiency, and the single-scattering phase function, determined with a ray-tracing approach for spheroidal particles (Macke & Mishchenko, 1996). Displayed simulation results correspond to a spheroid of minimum and maximum radii of 208 μm and 520 μm, respectively. The multiple scattering model was run for a solar zenith angle of 30° and increments of direct (*d*) and diffuse irradiance of *d*=1.0, 0.8, 0.6, 0.4, 0.2, and 0.0. These irradiance scenarios correspond to BRF and DHR for pure direct illumination conditions (*d*=1.0), and HDRF and BHR for the remaining.

#### 4.3.2. Results

In Fig. 8, we show the angular distributions of the irradiance scenarios for wavelength 0.55 μm. The models for *d*=1.0 through *d*=0.2 exhibit a forward reflectance distribution that decreases in magnitude with increasing diffuse component. For the totally diffuse irradiance scenario, the distribution shows a

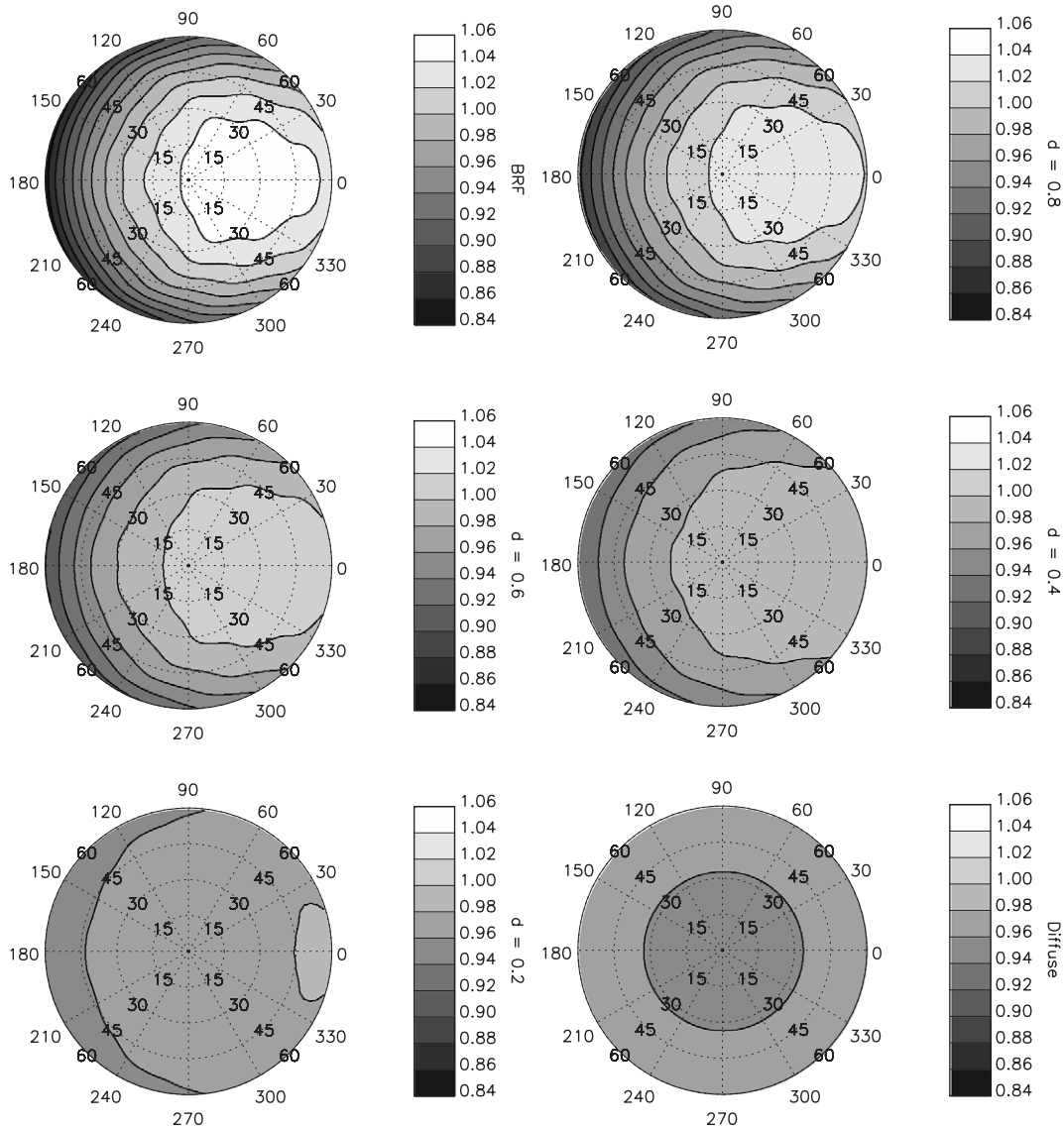


Fig. 8. Angular distribution of reflectance for a range of irradiance cases at 0.55 μm and solar zenith angle=30°. The target center represents the nadir view geometry  $\theta_r, \phi_r=(0^\circ, 0^\circ)$ , radial distance from center represents the view zenith angle, and the angle about the center represents the view azimuth angle. The forward reflectance direction is  $\phi_r=0^\circ$ .

shallow bowl shape. This minimum at nadir results from the angular intersection of the strong forward scattering phase function with the surface. The solar principal plane for these scenarios is given in Fig. 9 (top).

The differences at nadir between the BRF and HDRF at  $d=0.8$  and HDRF at  $d=0.6$  for  $\lambda=0.55 \mu\text{m}$  are 0.02 and 0.04, respectively, with maximum differences at view zenith angles of  $10^\circ$  to  $20^\circ$  in the forward direction. The bowl-shaped distribution for diffuse irradiance becomes relatively deeper at longer wavelengths (Fig. 9 (bottom)), such as  $1.03 \mu\text{m}$ . We show the  $1.03 \mu\text{m}$  model because this is the wavelength range in which snow reflectance is most sensitive to grain size and thus is used in imaging spectroscopy models for inference of grain size and albedo (Green et al., 2002; Nolin & Dozier, 2000). The enhancement of the bowl shape at greater diffuse irradiance is explained as above coupled with a decrease in the single-scattering albedo at the longer wavelengths. Only for the BRF and  $d=0.8$  irradiance cases is the distribution properly forward reflecting.

Fig. 10 shows DHR of snow relative to the illumination zenith angle with the associated BHR for isotropic diffuse illumination conditions. For both wavelengths, the DHR increases with increasing zenith angle but the increase is far greater in absolute and relative reflectance at  $1.03 \mu\text{m}$ .

**5. Conclusions**

The remote sensing community devotes major effort to calibration and validation of sensors, measurements, and de-

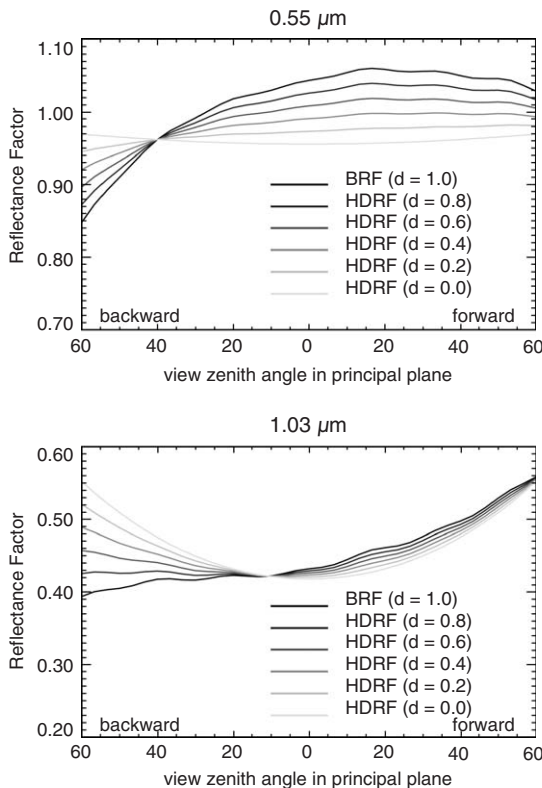


Fig. 9. Simulated BRF ( $d=1.0$ ) and HDRF ( $d=0.8$  to  $d=0.0$ ) data for snow in the solar principal plane at wavelengths  $0.55 \mu\text{m}$  (top) and  $1.03 \mu\text{m}$  (bottom).

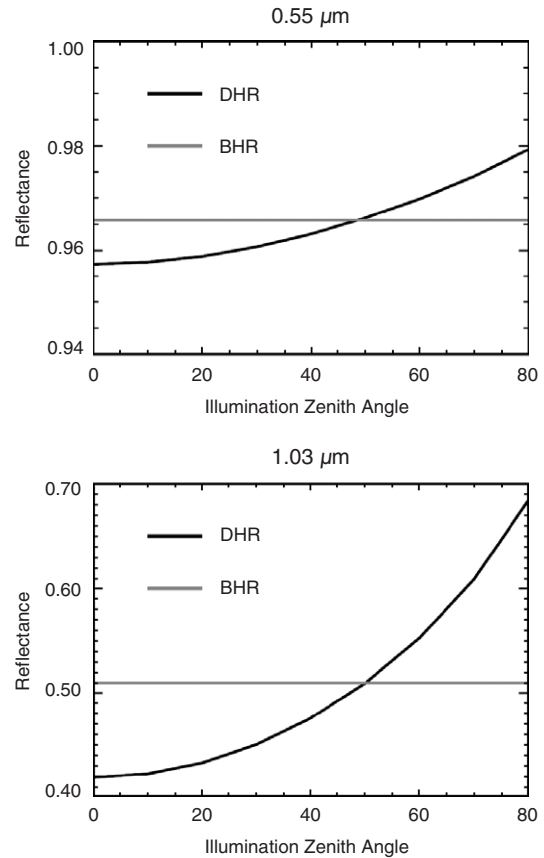


Fig. 10. Directional-hemispherical reflectance versus illumination zenith angle for snow at wavelengths  $0.55 \mu\text{m}$  and  $1.03 \mu\text{m}$ . The bihemispherical reflectance for isotropic diffuse illumination ( $d=0$ ) is included for comparison.

rired products to quantify and reduce their uncertainties. Given recent advances in instrument design, radiometric calibration, atmospheric correction, algorithm development, product development, validation, and delivery, the lack of standardization of reflectance terminology and products becomes a considerable source of error.

The variety in physical quantities resulting from different sensor sampling schemes, preprocessing, atmospheric correction, and angular modeling, requires a documentation standard for remotely sensed reflectance data. Beyond the algorithm theoretical basis document with a detailed description of the data processing, a short and standardized description on the physical character of the delivered reflectance products must be accessible by the user. This necessarily includes the accurate listing of opening angles and directions of illumination and observation used, revealing whether the product represents inherent reflectance properties of the surface or contains a diffuse illumination component corresponding to the atmospheric and terrain conditions of the observations.

Relying on this standardized reflectance description, users can then choose the reflectance products appropriate to their applications, depending on the coupling of the reflectance with the sky radiation. Inherent reflectance property data is available from few sensors only, but as shown by Pinty et al. (2005), crucial in, for example, climate modeling. Biases introduced by using an inappropriate reflectance quantity can exceed

minimum sensitivity levels of climate models (i.e.,  $\pm 0.02$  reflectance units (Sellers et al., 1995)), as shown by the comparison of different MISR reflectance products in this study. Further, they introduce systematic, wavelength dependent errors in reflectance and higher level product validation efforts, in data fusion approaches based on different sensors, and applications, where so-called ‘a priori BRDF knowledge’ is applied (Li et al., 2001). These differences are especially important in long-term, large area trend studies, as the latter are mostly based on multiple sensors with different angular sampling and modeling, as well as atmospheric correction schemes.

The selected examples from the peer-reviewed literature clearly show that the current use of reflectance terminology often does not comply with physical standards and has implications on scientific results. In order to stimulate users to choose the appropriate sensor and reflectance quantity and name it accordingly, they must have access to an easy to understand, physically based explanation of the delivered reflectance product.

After several decades of custom and practice using a vague reflectance terminology, it is important not to underestimate the efforts of standardization. Semantic interoperability and standardization for the benefit of the increasing base of remote sensing product customers has been recognized by various bodies and initiatives (e.g., ISPRS, GEO, GEOSS, INSPIRE, etc.), however the implementation will still take some time. With this paper, we contribute to the awareness and emphasize the importance of an ongoing discussion on reflectance terminology, trying to avoid multiple redevelopment of similar terminologies that would lead to a segregation of user communities. The same scrutiny and transparency applied to the peer-reviewed publication process should be applicable to reflectance data product providers, resulting in open standards facilitating data exchange and minimizing product uncertainties.

Future research should emphasize an integrated standardization of remote sensing data products, including the calibration process, the terminology of radiometric and photometric quantities used, as well as proper linkage of these products (e.g., various albedos) to physical models.

## Acknowledgement

The work of G. Schaepman-Strub was supported by the Swiss National Science Foundation (Project No. 200020-101517 and PBZH2-108485) and a European Space Agency’s External Fellowship. The MISR data were obtained from the NASA Langley Research Center Atmospheric Sciences Data Center. We thank Michel Verstraete for the discussion on an earlier version of the manuscript, and reviewers for their substantial comments.

## References

Asrar, G., & Myneni, R. (1993). Atmospheric effects in the remote sensing of surface albedo and radiation absorption by vegetation canopies. *Remote Sensing Reviews*, 7, 197–222.

Atzberger, C. (2004). Object-based retrieval of biophysical canopy variables using artificial neural nets and radiative transfer models. *Remote Sensing of Environment*, 93, 53–67.

Bacour, C., & Breon, F. M. (2005). Variability of biome reflectance directional signatures as seen by POLDER. *Remote Sensing of Environment*, 98, 80–95.

Breuer, L., Eckhardt, K., & Frede, H. G. (2003). Plant parameter values for models in temperate climates. *Ecological Modelling*, 169, 237–293.

Chopping, M. J. (2000). Testing a LiSK BRDF model with in situ bidirectional reflectance factor measurements over semiarid grasslands. *Remote Sensing of Environment*, 74, 287–312.

Copernicus, N. (1543). *De revolutionibus orbium coelestium libri sex*.

Dangel, S., et al. (2005). Toward a direct comparison of field and laboratory goniometer measurements. *IEEE Transactions on Geoscience and Remote Sensing*, 43, 2666–2675.

Deering, D. W., et al. (1995). Temporal attributes of the bidirectional reflectance for three boreal forest canopies. *IGARSS* (pp. 1239–1241). Piscataway, NJ, United States: IEEE.

Deering, D. W., & Eck, T. F. (1987). Atmospheric optical depth effects on angular anisotropy of plant canopy reflectance. *International Journal of Remote Sensing*, 8, 893–916.

Deering, D. W., Eck, T. F., & Otterman, J. (1990). Bidirectional reflectances of selected desert surfaces and their 3-parameter soil characterization. *Agricultural and Forest Meteorology*, 52, 71–93.

Deering, D. W., & Leone, P. (1986). A sphere-scanning radiometer for rapid directional measurements of sky and ground radiance. *Remote Sensing of Environment*, 19, 1–24.

Di Girolamo, L. (2003). Generalizing the definition of the bi-directional reflectance distribution function. *Remote Sensing of Environment*, 88, 479–482.

Diner, D. J., et al. (1999). *Multi-angle imaging spectro-radiometer level 2 surface retrieval algorithm theoretical basis*. JPL D-11401, Rev. D, December 2, 1999. Jet Propulsion Laboratory, California Institute of Technology.

Dozier, J. (1980). A clear-sky spectral solar-radiation model for snow-covered mountainous terrain. *Water Resources Research*, 16, 709–718.

Engelsen, O., et al. (1996). Parametric bidirectional reflectance factor models: Evaluation, improvements and applications. *Tech. Rep. EUR 16426 EN* (pp. 114). Ispra, Italy: EC Joint Research Centre.

Fang, H., et al. (2004). Statistical comparison of MISR, ETM plus and MODIS land surface reflectance and albedo products of the BARC land validation core site, USA. *International Journal of Remote Sensing*, 25, 409–422.

Friedl, M. A., et al. (2002). Global land cover mapping from MODIS: Algorithms and early results. *Remote Sensing of Environment*, 83, 287–302.

Gingerich, O. (2004). *The book nobody read*. New York: Walker and Company.

Grant, I. F., Breon, F. M., & Leroy, M. M. (2003). First observation of the hot spot from space at sub-degree angular resolution using POLDER data. *International Journal of Remote Sensing*, 24, 1103–1110.

Green, R. O., et al. (2002). Spectral snow-reflectance models for grain-size and liquid–water fraction in melting snow for the solar-reflected spectrum. *Annals of Glaciology*, 34, 71–73.

Kimes, D. S. (1983). Dynamics of directional reflectance factor distributions for vegetation canopies. *Applied Optics*, 22, 1364–1372.

Kipp, & Zonen (2000). *Instruction manual CM11 Pyranometer/CM14 Albedometer* (pp. 65). Delft, The Netherlands: Kipp and Zonen.

Koehler, C., et al. (1994). The European optical goniometric facility: Technical description and first experiments on spectral unmixing. *IGARRS’94* (pp. 2375–2377). USA: Pasadena.

Koestler, A. (1959). *The sleepwalkers*. London: Hutchinson.

Koetz, B., et al. (2004). Radiative transfer modeling within a heterogeneous canopy for estimation of forest fire fuel properties. *Remote Sensing of Environment*, 92, 332–344.

Kriebel, K. T. (1976). On the variability of the reflected radiation field due to differing distributions of the irradiation. *Remote Sensing of Environment*, 4, 257–264.

Kriebel, K. T. (1978). Average variability of radiation reflected by vegetated surfaces due to differing irradiances. *Remote Sensing of Environment*, 7, 81–83.

Lee, T. Y., & Kaufman, Y. J. (1986). Non-Lambertian effects on remote-sensing of surface reflectance and vegetation index. *IEEE Transactions on Geoscience and Remote Sensing*, 24, 699–708.

- Lewicki, S., et al. (2003). *MISR data products specifications—Incorporating the science data processing interface control document, MISR DPS, JPL D-13963, Revision 1, July, 2003*. URL: <http://eosweb.larc.nasa.gov/PRODOCS/misr/Version/pge9.html>
- Lewis, P., & Barnsley, M. J. (1994). Influence of the sky radiance distribution on various formulations of the earth surface albedo. *6th International Symposium on Physical Measurements and Signatures in Remote Sensing, ISPRS* (pp. 707–715). Val d'Isere, France: CNES.
- Li, X. W., et al. (2001). A priori knowledge accumulation and its application to linear BRDF model inversion. *Journal of Geophysical Research-Atmospheres*, *106*, 11925–11935.
- Liang, S. L., Fang, H. L., & Chen, M. Z. (2001). Atmospheric correction of landsat ETM+ land surface imagery: Part I. Methods. *IEEE Transactions on Geoscience and Remote Sensing*, *39*, 2490–2498.
- Liu, C. H., Chen, A. J., & Liu, G. R. (1994). Variability of the bare soil albedo due to different solar zenith angles and atmospheric haziness. *International Journal of Remote Sensing*, *15*, 2531–2542.
- Lucht, W., Schaaf, C. B., & Strahler, A. H. (2000). An algorithm for the retrieval of albedo from space using semiempirical BRDF models. *IEEE Transactions on Geoscience and Remote Sensing*, *38*, 977–998.
- Lyapustin, A. I., & Privette, J. L. (1999). A new method of retrieving surface bidirectional reflectance from ground measurements: Atmospheric sensitivity study. *Journal of Geophysical Research-Atmospheres*, *104*, 6257–6268.
- Macke, A., & Mishchenko, M. I. (1996). Applicability of regular particle shapes in light scattering calculations for atmospheric ice particles. *Applied Optics*, *35*, 4291–4296.
- Martonchik, J. V. (1994). Retrieval of surface directional reflectance properties using ground-level multiangle measurements. *Remote Sensing of Environment*, *50*, 303–316.
- Martonchik, J. V., Bruegge, C. J., & Strahler, A. (2000). A review of reflectance nomenclature used in remote sensing. *Remote Sensing Reviews*, *19*, 9–20.
- Martonchik, J. V., et al. (1998). Determination of land and ocean reflective, radiative, and biophysical properties using multiangle imaging. *IEEE Transactions on Geoscience and Remote Sensing*, *36*, 1266–1281.
- Nicodemus, F. E. (1965). Directional reflectance and emissivity of an opaque surface. *Applied Optics*, *4*, 767–773.
- Nicodemus, F. E., et al. (1977). *Geometrical considerations and nomenclature for reflectance*. Washington, DC: National Bureau of Standards, US Department of Commerce. URL: <http://physics.nist.gov/Divisions/Div844/facilities/specphoto/pdf/geoConsid.pdf>
- Nolin, A. W., & Dozier, J. (2000). A hyperspectral method for remotely sensing the grain size of snow. *Remote Sensing of Environment*, *74*, 207–216.
- Nolin, A. W., & Liang, S. (2000). Progress in bidirectional reflectance modeling and applications for surface particulate media: Snow and soils. *Remote Sensing Reviews*, *18*, 307–342.
- Painter, T. H., & Dozier, J. (2004). Measurements of the hemispherical-directional reflectance of snow at fine spectral and angular resolution. *Journal of Geophysical Research-Atmospheres*, *109*.
- Painter, T. H., Paden, B., & Dozier, J. (2003). Automated spectro-goniometer: A spherical robot for the field measurement of the directional reflectance of snow. *Review of Scientific Instruments*, *74*, 5179–5188.
- Palmer, J. M. (1999). Radiometry and photometry FAQ. URL: <http://www.optics.arizona.edu/Palmer/rpfag/rpfag.htm#motivation>
- Peltoniemi, J. I., et al. (2005). BRDF measurement of understory vegetation in pine forests: dwarf shrubs, lichen, and moss. *Remote Sensing of Environment*, *94*, 343–354.
- Pinty, B., et al. (2005). Coupling diffuse sky radiation and surface albedo. *Journal of the Atmospheric Sciences*, *62*, 2580–2591.
- Rahman, H., Pinty, B., & Verstraete, M. M. (1993). Coupled surface-atmosphere reflectance (Csar) Model: 2. Semiempirical surface model usable with NOAA advanced very high-resolution radiometer data. *Journal of Geophysical Research-Atmospheres*, *98*, 20791–20801.
- Ranson, K. J., Biehl, L. L., & Bauer, M. E. (1985). Variation in spectral response of soybeans with respect to illumination, view and canopy geometry. *International Journal of Remote Sensing*, *6*, 1827–1842.
- Richter, R., & Schlapfer, D. (2002). Geo-atmospheric processing of airborne imaging spectrometry data: Part 2. Atmospheric/topographic correction. *International Journal of Remote Sensing*, *23*, 2631–2649.
- Roberts, D. A., Smith, M. O., & Adams, J. B. (1993). Green vegetation, non-photosynthetic vegetation, and soils in AVIRIS data. *Remote Sensing of Environment*, *44*, 255–269.
- Russell, P. B., et al. (1993). Pinatubo and pre-Pinatubo optical-depth spectra—Mauna-Loa measurements, comparisons, inferred particle-size distributions, radiative effects, and relationship to lidar data. *Journal of Geophysical Research-Atmospheres*, *98*, 22969–22985.
- Sandmeier, S. R., & Itten, K. I. (1999). A field goniometer system (FIGOS) for acquisition of hyperspectral BRDF data. *IEEE Transactions on Geoscience and Remote Sensing*, *37*, 978–986.
- Sellers, P. J., et al. (1995). Remote-sensing of the land-surface for studies of global change—models, algorithms, experiments. *Remote Sensing of Environment*, *51*, 3–26.
- Snyder, W. C. (2002). Definition and invariance properties of structured surface BRDF. *IEEE Transactions on Geoscience and Remote Sensing*, *40*, 1032–1037.
- Stamnes, K., et al. (1988). Numerically stable algorithm for discrete-ordinate-method radiative-transfer in multiple-scattering and emitting layered media. *Applied Optics*, *27*, 2502–2509.
- Strub, G., et al. (2003). Evaluation of spectrodirectional Alfalfa canopy data acquired during DAISEX'99. *IEEE Transactions on Geoscience and Remote Sensing*, *41*, 1034–1042.
- Susaki, J., et al. (2004). Validation of temporal BRDFs of paddy fields estimated from MODIS reflectance data. *IEEE Transactions on Geoscience and Remote Sensing*, *42*, 1262–1270.
- Tanre, D., Herman, M., & Deschamps, P. Y. (1983). Influence of the atmosphere on space measurements of directional properties. *Applied Optics*, *22*, 733–741.
- Vermote, E. F., & Vermeulen, A. (1999). *Atmospheric correction algorithm: Spectral reflectances (MOD09), MODIS ATBD* (pp. 107). : Dept. of Geography, University of Maryland.